



## Numerical Investigation of Nonlinear Oscillations and Compression-Only Behavior of a Coated Microbubble Near an Elastic Wall

S. B. Hosseini, M. Mahdi\*

*Mechanical Engineering Department, Shahid Rajaei Teacher Training University, Tehran, Iran*

### PAPER INFO

#### Paper history:

Received 15 June 2020  
Received in revised form 09 July 2020  
Accepted 17 August 2020

#### Keywords:

*Compression-Only Behavior  
Elastic Wall  
Nonlinear Oscillations  
Subharmonic Component  
Ultrasound Contrast Agents*

### ABSTRACT

During the ultrasound imaging process, the ultrasound contrast agents (UCAs) are beating near the blood vessel wall. Therefore, the purpose of the present simulation study is to investigate the effect of the presence of an elastic wall on the radial and frequency acoustic response of a UCA microbubble oscillating in a nonlinear regime. For this reason, the numerical simulation of the dynamic behavior of a coated microbubble was performed using coding in MATLAB and a Rayleigh-Plesset equation modified by Doinikov. To study the nonlinear bubble oscillations, its compression-only behavior and the subharmonic nonlinear component are taken from a nonlinear shell model presented by Marmottant et al. Initially, coated bubble oscillations in two linear and nonlinear regimes were investigated for two types of shell models, and it was observed that presence of the elastic wall affects the bubble's compression-only behavior. Finally, due to the importance of the subharmonic component in the nonlinear oscillation of the coated bubble, the threshold of the appearance of subharmonic components for a coated bubble near an elastic wall was investigated using the Fast Fourier Transform (FFT) and compared with the oscillation in the infinite fluid.

doi: 10.5829/ije.2020.33.10a.28

## 1. INTRODUCTION

The mechanism of diagnostic imaging in medicine by ultrasound is based on the scattering and reflection of the ultrasound waves sent from the target tissue. Unlike body tissues, the scattering properties of blood are very poor and ultrasound transmitted waves attenuate after reflection and reduce imaging quality due to the low reflection of blood and some tissues against ultrasound waves which either absorb or transmit the ultrasound waves. To increase the reflectance of ultrasound beams, micrometer coated bubbles (ultrasound contrast agents) that are covered by a stabilizing shell (a variety of proteins such as lipid or albumin) are intravenously injected. These contrast agent microbubbles due to their oscillations prevent the wave attenuation, and increase the acoustic differentiation between blood and tissue during an ultrasound examination and improve image quality. The UCA microbubbles usually have a small size

of about microns (1 to 10 micrometers) that enables them to pass through the smallest capillaries in the body. Bubble coating has been done to increase the stability of the free bubbles, prevent its rapid dissolution, and prevent their agglomeration which has led to the production of different generations of UCA bubbles. Adding a special coating with a certain viscosity and elasticity to the free bubbles alters the surface tension of the bubbles and consequently changes their acoustic behavior dramatically. In medical applications, UCA microbubbles move near boundary surfaces such as the wall of a laboratory container or the wall of a blood vessel. Therefore, the theoretical models that predict the effect of a wall on the dynamics of a UCA microbubble are interesting. Studying this information is important for determining the imaging methods and the microbubble parameters owing to their ability to optimize imaging clarity, improve imaging quality, and assist the development of new imaging strategies.

\*Corresponding Author Institutional Email: [M.mahdi@sru.ac.ir](mailto:M.mahdi@sru.ac.ir)  
(M. Mahdi)

The dynamics of the bubble in an ultrasonic field is described by the Rayleigh-Plesset (RP) equation, but the addition of a shell to the bubble and the presence of a wall near the bubble will change the above equation. To study the dynamics of the coated bubble, De Jong et al. [1] presented the first models and parameters (shell friction and shell elasticity) to determine the coating effects. Church et al. [2] developed the first accurate model of coating theory by a layer of incompressible rubber material using a Modified Rayleigh-Plesset equation. Hoff et al. [3] used a thin-shell model of polymer and observed that this coating increases the bubble shell resistance by up to 20 times compared to the free gas bubble. Later, De Jong et al. [4] investigated the response of the UCA in nonlinear regimes appearing at high pressures and observed that nonlinear bubble oscillations produce harmonics and sub-harmonics in the bubble behavior.

Several researchers like Brennen [5], Leighton [6], and Blake and Gibson [7] investigated the dynamics of a free gas bubble near a solid boundary. In medical imaging, bubbles may be in the proximity of the vessel or capillary that will therefore affect the pressure propagated from the bubble. It has provided a motivation for studying the effect of a boundary on a coated bubble. For the first time, Herring [8] made numerical study of the free bubble near the wall. Then, Strasberg [9] and Blue [10] examined the effect of a rigid wall on the resonant frequency of a free bubble. In their assumptions, the interaction of a bubble with a rigid boundary is mathematically equivalent to the interaction between two pulsating, in-phase, and adjacent bubbles. Since then, this equivalence has been utilized in many studies, such as the study reported by Doinikov et al. [11], to investigate the dynamical behavior of bubbles. Tomita and Shima [12] also presented a modified Rayleigh-Plesset equation for a free bubble that incorporated the rigid wall effects and the compressibility of the fluid around the bubble. This equation, developed by the Image Source Method, was used by Doinikov et al. [13] to derive a modified Rayleigh-Plesset equation for a bubble near a fluid layer of finite thickness. Experimental data show that the proximity of a boundary to the bubble and the mechanical properties of the material of the shell can cause significant changes in the amplitude of the micro bubble's oscillation and its propagated pressure [14]. Many theoretical studies predicted that the resonance frequency of a UCA near a boundary can be reduced or increased depending on the mechanical properties of the boundary [15]. In an experimental work, Garbin et al. [14] observed that the oscillation amplitude of a BR-14 microbubble near the wall of an OptiCell chamber is suppressed by more than 50%.

These findings prompted scientists to focus on the interaction of the UCA microbubbles and the ultrasound

waves, and the effect of vessel wall proximity to have a better understanding of its behavior in an ultrasound field. Various modeling studies have been conducted to understand the bubble response when it passes along the vessel wall. Primary studies such as that reported by Leighton [6] investigated the response of the bubble near the rigid wall of the vessel. However, the recent studies indicate the need for a comprehensive understanding of the more flexible boundaries effect because these boundaries are biologically more important. Doinikov et al. [11] modeled the UCA microbubbles responses using the modified Rayleigh-Plesset equation near the rigid wall and analyzed it. Overvelde et al. [16] investigated the presence of a rigid wall and its effect on the behavior of the UCA microbubbles. They found that, in particular, the resonance frequency of the microbubbles and the intensity of the scattered pressure field varied, so that the maximum resonance frequency of the bubble attached to the wall was 50% lower than the bubble in the infinite fluid. Doinikov et al. [13] investigated the oscillating UCA responses near a thin layer of finite density. They attempted to develop a new theoretical model to investigate the effects of the layer thickness and density on the pressure field scattered from the bubble. In 2013, Aired et al. [17] investigated the dynamics of the coated bubble near three different types of the wall, two different distances from the wall, and three different initial radii. They studied the changes of fundamental and second harmonic frequencies. Garashchuk et al. [18] also considered different models of coated bubbles and investigated their multi-dynamic stability and the occurrence of complex three-dimensional nonlinear dynamics. Dvinikov et al. [15] investigated the interaction of bubbles and walls at arbitrary distances to complete their earlier theory. Their simulation results showed that the bubble resonance frequency near the wall is dependent on the distance from the wall and the elastic properties of the wall.

In the present study, a Rayleigh-Plesset equation modified by Doinikov is used to simulate the UCA microbubble behavior near an elastic wall of finite thickness to investigate how the elastic wall proximity affects the microbubble behavior and the acoustic response of the microbubble. Therefore, for the first time, for a coated bubble near an elastic wall with finite thickness, the occurrence of the nonlinear oscillations and its resulting components (such as harmonic components and compression-only behavior) have been simulated. Due to the importance of nonlinear bubble oscillations in medical applications, the focus of this paper is on the nonlinear behavior of the UCA microbubble near an elastic wall. The bubble oscillation behavior is simulated using the fourth-order Runge-Kutta method and the Doinikov equation and is compared with the experimental results.

## 2. THEORY

Up to now, several types of Rayleigh-Plesset equations have been derived for coated bubbles, but for a coated bubble several factors influence its dynamic behavior (including the presence of a wall near the bubble). Today, there are varieties of ultrasound medical technologies that use UCAs, in which, the microbubble interactions occur with different boundaries. In clinical applications, such as ultrasound imaging, these boundaries could be the blood vessel wall, while in the laboratory applications could be the wall of laboratory containers made of various materials.

### 2. 1. Coated Bubble in Infinite Fluid and Near an Elastic Wall

Almost all the mathematical models of microbubble dynamics are based on modifications of the Rayleigh-Plesset equation, which is for the growth and collapse of a gas bubble and can be expressed in a new context. Assuming a polytropic law for bubble gas and regardless of the vapor pressure inside the bubble, the following form of the modified Rayleigh-Plesset equation can be used to model the dynamics of coated microbubbles in an infinite fluid [19]:

$$\rho_l \left[ R\ddot{R} + \frac{3}{2}\dot{R}^2 \right] = \left( P_0 + \frac{2\sigma(R_0)}{R_0} \right) \left( \frac{R_0}{R} \right)^{3k} \left( 1 - \frac{3k\dot{R}}{c} \right) - \frac{2\sigma(R)}{R} - \frac{4\mu\dot{R}}{R} - \frac{4\dot{R}}{R^2} K_s(R, \dot{R}) - P_0 - P_{ac}(t) \quad (1)$$

where  $R$  is the bubble radius,  $R_0$  the initial bubble radius,  $k$  the ratio of specific heats of the gas,  $P_0$  the hydrostatic ambient pressure,  $\mu$  the fluid viscosity,  $\sigma(R)$  the effective surface tension of the bubble,  $c$  the speed of sound at ambient,  $\rho$  the density of the surrounding liquid,  $K_s$  the shell viscosity and  $P_{ac}(t)$  the external excitation pressure applied to the bubble. To model the pressure field scattered from the bubble in an infinite fluid, one obtains [19]:

$$P_{scater}(r, t) = \frac{\rho_l R}{r} (R\ddot{R} + 2\dot{R}^2) \quad (2)$$

where  $P_{scater}$  is the scattered pressure from the bubble and  $r$  the measured distance from the center of the bubble [20]. Nevertheless, the theoretical models that predict the effect of a wall on the dynamics of a coated microbubble receive much attention, because, in medical applications (laboratory, therapeutic, and imaging), the UCA microbubbles move near different boundary surfaces.

Figure 1 shows a schematic of a coated bubble near an elastic wall of finite thickness. The bubble is at a distance  $d$  from the wall (environment 2) and  $h$  is the thickness of the wall. The wall material is assumed to be an elastic solid with a density of  $\rho_2$ , a bulk modulus  $K_{wall}$ , and a shear modulus  $\mu_{wall}$ . The back wall environment is also assumed to be an ideal and incompressible fluid with a density of  $\rho_3$ .

Because the presence of a wall affects the behavior of the UCA microbubbles, Doinikov et al. [13] developed a

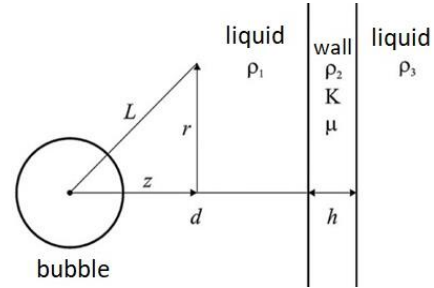


**Figure 1.** Schematic of a bubble near an elastic wall with finite thickness

modified Rayleigh-Plesset family of equation for a coated microbubble near an elastic wall of finite thickness to investigate the effect of the presence of a wall on the UCA microbubble acoustic response. These equations are as follows [13]:

$$\ddot{R}R(1 - \alpha) + \frac{3}{2}\dot{R}^2 \left( 1 - \frac{4\alpha}{3} \right) = \frac{1}{\rho_l} \left[ \left( P_0 + \frac{2\sigma}{R_0} \right) \left( \frac{R_0^3 - a^3}{R^3 - a^3} \right)^{\gamma} - \frac{2\sigma(R)}{R} - 4\mu \frac{\dot{R}}{R} - P_0 - P_{ac}(t) - S \right] \quad (3)$$

The variable  $\alpha$  is as follows [13]:

$$\alpha = \frac{(\rho_1 - \beta)R}{(\rho_1 + \beta)2h} - \frac{(\beta - \rho_2)R}{(\beta + \rho_2)2(h+t)} + \frac{(\rho_1 - \beta)(\beta - \rho_2)R}{(\rho_1 + \beta)(\beta + \rho_2)2t} \quad (4)$$

Equation (3) neglects the radiation damping due to the liquid compressibility. This effect can be taken into account by one of the most common modified Rayleigh-Plesset equations for compressible fluids such as Keller-Miksis equation. These equations are as follows [13]:

$$\ddot{R}R \left( 1 - \alpha - \frac{\dot{R}}{c} \right) + \frac{3}{2}\dot{R}^2 \left( 1 - \frac{4\alpha}{3} - \frac{\dot{R}}{3c} \right) = \frac{1}{\rho_l} \left( 1 + \frac{\dot{R}}{c} + \frac{R}{c} \frac{d}{dt} \right) \left[ \left( P_0 + \frac{2\sigma}{R_0} \right) \left( \frac{R_0^3 - a^3}{R^3 - a^3} \right)^{\gamma} - \frac{2\sigma(R)}{R} - 4\mu \frac{\dot{R}}{R} - P_0 - P_{ac}(t) - S \right] \quad (5)$$

where  $S$  is the term describing shell effect and  $a$  is the radius of the bubble's van der Waals hard core. The acoustic pressure wave scattered from the coated bubble near an elastic wall at  $L$  distance from the center of the bubble is as follows [13]:

$$P_{scater} = \frac{\rho_l(R^2\ddot{R} + 2R\dot{R}^2)}{L} \left[ 1 - \frac{(\rho_1 - \beta)}{(\rho_1 + \beta)} \frac{L}{\sqrt{L^2 + 4d^2 - 4dz_1}} - \frac{(\beta - \rho_3)}{(\beta + \rho_3)} \frac{L}{\sqrt{L^2 + 4(d+h)^2 - 4(d+h)z_1}} + \frac{(\rho_1 - \beta)(\beta - \rho_3)}{(\rho_1 + \beta)(\beta + \rho_3)} \frac{L}{\sqrt{L^2 + 4h^2 - 4hz_1}} \right] \quad (6)$$

If  $L$  is large compared to  $d$  and  $h$ , Equation (6) can be rewritten as follows [13]:

$$P_{scater} = \frac{\rho_l(R^2\ddot{R} + 2R\dot{R}^2)}{L} \frac{4\beta\rho_3}{(\rho_1 + \beta)(\beta + \rho_3)} \quad (7)$$

After that, in 2013, Aired et al. [17] considered some modifications to improve an equation for the coated bubble dynamics near an elastic wall using the De Jong shell as follows [13]:

$$\begin{aligned} \dot{R}R(1-\alpha) + \frac{3}{2}\dot{R}^2\left(1-\frac{4\alpha}{3}\right) = & \left[ P_0 + \right. \\ \frac{2\sigma}{R_0}\left(\frac{R_0}{R}\right)^{3\gamma}\left(1-\frac{3\gamma}{c}\dot{R}\right) - \frac{2\sigma(R)}{R} - 4\mu\frac{\dot{R}}{R} - P_0 - & \\ P_{ac}(t) - 4\chi\left(\frac{1}{R_0} - \frac{1}{R}\right) - \frac{4K_s\dot{R}}{R^2} & \left. \right] \end{aligned} \quad (8)$$

where  $K_s$  and  $\chi$  are shell viscosity and shell elasticity, respectively. Marmottant et al [21] also introduced a shell model that is suitable for high amplitude oscillations. This model assumes an elastic shell with buckling and rupture states. Three important factors are involved in the performance of this shell model.

1-the buckling radius which plays a major role in predicting the compression-only behavior, 2-the compressibility of the shell material and 3-the rupture radius which plays the major role in predicting the disappearance of compression-only behavior [19–22].

$$\begin{aligned} & 0 & R \leq R_{buckling} \\ \sigma(R) = & \chi\left(\frac{R^2}{R_{buckling}^2} - 1\right) & R_{buckling} \leq R \\ & & \& R \leq R_{rupture} \\ & \sigma_{water} & R \geq R_{rupture} \end{aligned} \quad (9)$$

$$K_s(R) = K_s$$

$$f_0 = \frac{1}{2\pi R_0} \sqrt{\frac{1}{\rho}\left(3\gamma P_0 + \frac{4\sigma(R_0)}{R_0}(3\gamma - 1) + \frac{4\chi}{R_0}\right)} \quad (10)$$

And the critical radius of this model is as follows [21]:

$$R_{rupture} = R_{buckling}(1 + \sigma_{water}/\chi)^{1/2} \quad (11)$$

$$R_{buckling} = R_0(1 + \sigma(R_0)/\chi)^{-1/2} \quad (12)$$

In the Marmottant model, the effective surface tension operates within a certain range; for the values more than  $R_{rupture}$  the bubble behaves like a free gas bubble, and for the values less than  $R_{buckling}$  the bubble shell folds. For the latter, the effective surface tension is considered to be zero.

**2.2. Validation of Numerical Model** In section 2.2, the numerical outputs are validated with experimental results to ensure the accuracy of the simulation results. First, by using the Rayleigh-Plesset model, the dynamics of a free bubble is simulated, and then by using the modified Rayleigh-Plesset improved by Doinikov for the coated bubbles, the dynamics of a coated bubble is simulated. Figure 2 is obtained using the experimental results by Lofstedt et al. [22], and Figure 3 is established using the experimental results by Garbin et al. [14]. The latter authors had recorded the dynamic behavior of a coated bubble by high-speed cameras near an elastic wall. In the validation section, the excitation pulse is applied as a Gaussian pulse with the frequency and amplitude according to the experimental conditions.

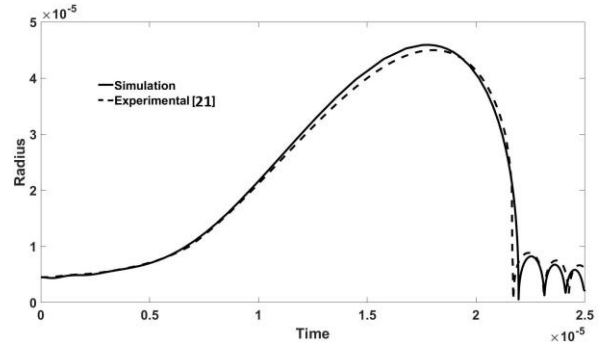


**Figure 2.** Validation of numerical solution and the experimental data for radial oscillation of a free bubble (Rayleigh–Plesset equation), ( $R_0 = 1.6\mu\text{m}$ ,  $P_a = 0.2\text{ MPa}$ ,  $f = 2\text{ MHz}$ )

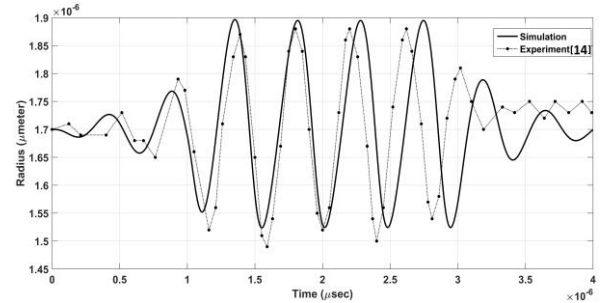


**Figure 3.** Validation of numerical solution and the experimental data for radial oscillation of an encapsulated bubble near an elastic wall (modified Rayleigh–Plesset equation by Doinikov), ( $R_0 = 1.7\mu\text{m}$ ,  $P_a = 58\text{ KPa}$ ,  $f = 2.5\text{ MHz}$ ,  $\chi = 0.32\text{ N/m}$ ,  $K_s = 2.10^{-9}\text{ kg/s}$ ,  $d = 100\mu\text{m}$ )

It can be seen from Figure 3 that both numerical and experimental results oscillate around the equilibrium radius of  $1.7\mu\text{m}$  with the same trend and at the top of the graph, there is an average difference of 0.6% in amplitude. It is also observed that the numerical results predict the process of changing the oscillatory, compression, and expansion behavior of the bubble are well in accordance with the experimental results. The fourth-order Runge-Kutta method has been used for simulation. This method has been used due to resistance to divergence and stiff problems. Validations were performed under the following physical conditions (for Figure 3) [14]:

$$\begin{aligned} R_0 &= 1.7\ (\mu\text{m}) & \gamma &= 1.07 & \sigma_L &= 0.072\ (\text{N/m}) \\ K_s &= 0.72e^{-8}\ (\text{Kg/s}) & d &= 50\ (\mu\text{m}) & \chi &= 0.51\ (\text{N/m}) \\ \mu_L &= 0.001\ (\text{Pa}\cdot\text{s}) & P_a &= 200\ (\text{KPa}) & P_a &= 200\ (\text{KPa}) \\ P_0 &= 101325\ (\text{Pa}) & h &= 75\ (\mu\text{m}) & c &= 1500\ (\text{m/s}) \\ \rho_L &= 1000\ (\text{kg/m}^{-3}) & \rho_{wall} &= 1060\ (\text{kg/m}^{-3}) \\ P_{ac}(t) &= P_a \sin(2\pi ft) \exp\left[-\left(\frac{2ft}{N}\right)^4\right] \end{aligned}$$

Besides, the numerical outputs in the field of frequency response are validated by comparing with the experimental results. Figures 4 and 5 are presented by

applying a Marmottant nonlinear shell model to the coated bubble dynamic equation and then by employing Equation (7). By applying Fast Fourier Transform (FFT) on the pressure wave propagated from the bubble, the frequency responses of the fundamental and subharmonic components are obtained and compared with the experimental results by Paul et al. [19]. Validations were performed under the following physical conditions (for Figures 4 and 5) [19]:

$$\begin{aligned} R_0 &= 1.6 \text{ (}\mu\text{m)} & P_0 &= 101325 \text{ (Pa)} & \gamma &= 1.07 \\ K_s &= 1.2e^{-8} \text{ (Kg/s)} & \chi &= 0.51 \text{ (N/m)} & c &= 1500 \text{ (m/s)} \\ \mu_L &= 0.001 \text{ (Pa.s)} & P_a &= 1.6 \text{ (MPa)} & f &= 3 \text{ (MHz)} \\ \rho_L &= 1000 \text{ (kg/m}^{-3}\text{)} & \sigma_L &= 0.072 \text{ (N/m)} & & \\ P_{ac}(t) &= P_a \sin(2\pi ft) & & & & \end{aligned}$$

Figure 6 shows the frequency response spectrum emitted from a coated bubble using a Marmottant nonlinear shell model.

### 3. DISCUSSION

When the bubble is excited by an acoustic pulse, the pressure waves are propagated by the bubble oscillation. The wave propagated by the bubble may have different frequency components depending on the intensity of the

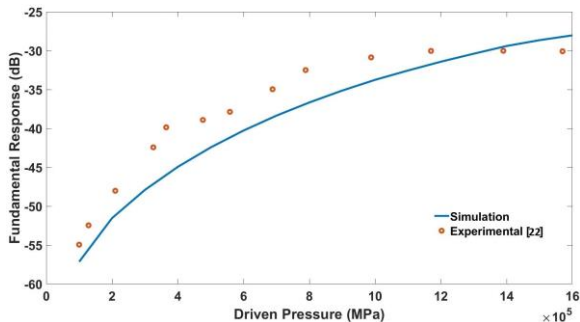


**Figure 4.** Validation of numerical solution and the experimental data for fundamental response of Sonazoid bubble ( $f = 3$  MHz)

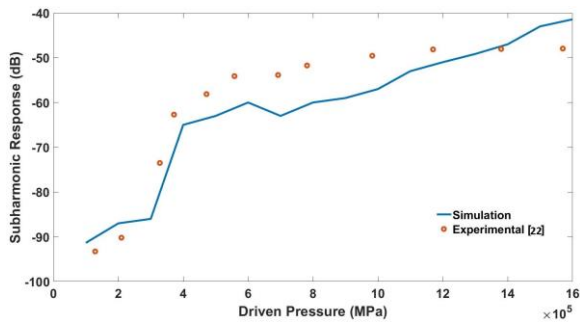


**Figure 5.** Validation of numerical solution and the experimental data for subharmonic response of Sonazoid bubble ( $f = 3$  MHz)

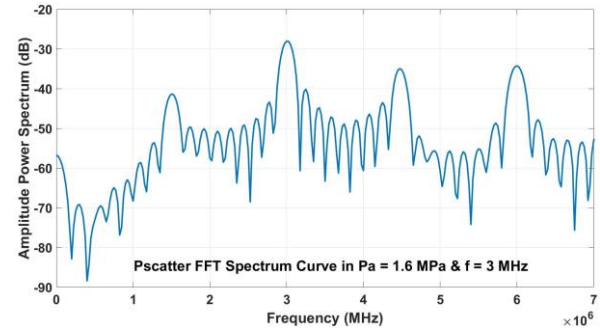


**Figure 6.** Frequency spectrum of a Sonazoid bubble ( $P_a = 1.6$  MPa,  $f = 3$  MHz)

excitation. In this scattered pressure wave from the bubble, there is always a fundamental component which is the frequency of excitation of the bubble. As the excitation intensity increases, the higher harmonic components, which are integer coefficients of the fundamental component (such as  $nf_i$ ), can also appear in the Fourier spectrum of the bubble frequency responses. As the excitation pulse intensities increase, nonlinear components, such as sub-harmonic and ultra-harmonic components, also appear in the pressure spectrum scattered from the bubble, where the sub-harmonic components are as the coefficient of  $1/2f_i$ , and the ultra-harmonic components are as the coefficient of  $2.3f_i$ . As the excitation pulse intensities increase, the bubble oscillation frequency response spectrum enters the saturation phase with severe noises. The nonlinear components are integrated into these noises and are no longer detectable. Since the wave propagated from the bubble contains a set of mentioned above frequencies, it is therefore necessary to extract and analyze each of these waves by applying the Fourier series to the time domain transfer. The current simulation study aims to show how the presence of an elastic boundary affects the radial and frequency response of a UCA bubble in a nonlinear oscillatory regime. The bubble and shell properties used in the numerical simulation are listed in Table 1. Simulations were performed under the following physical conditions [13]:

$$\begin{aligned} \mu_L &= 0.001 \text{ (Pa.s)} & \sigma_L &= 0.072 \text{ (N/m)} & \gamma &= 1.07 \\ \mu_{wall} &= 1.34 \text{ (GPa)} & P_0 &= 101325 \text{ (Pa)} & d &= 2R_0 \\ \rho_L &= 1000 \text{ (kg/m}^{-3}\text{)} & K &= 3.75 \text{ (GPa)} & R_0 &= 1.6 \text{ (}\mu\text{m)} \\ \rho_{wall} &= 1060 \text{ (kg/m}^{-3}\text{)} & c &= 1500 \text{ (m/s)} & h &= 75 \text{ (}\mu\text{m)} \end{aligned}$$

In the simulation steps, the excitation pulse is applied as a burst sinusoidal pulse with a specified frequency and amplitude.

**TABLE 1.** Marmottant Model Parameters [21]

$K_s$ (Kg/s)	$\chi$ (N/m)
$1.2 \times 10^{-8}$	0.53

### 3. 1. Investigation of the Nonlinear Bubble Oscillation and Compression-only Behavior Near an Elastic Wall

The coated bubble oscillations are linear or nonlinear depending on the magnitude of their excitation pressure. In the low excitation amplitudes, the behavior of the coated bubble is quite linear and does not affect the nonlinear factors in the radius-time graph and its frequency response spectrum. Most of the linear shell models presented for the linear oscillations assume a bubble surface tension as a constant number, but, at higher excitation pressure amplitudes, the coated microbubble behavior tends to become nonlinear. Therefore, the nonlinear factors will appear in the radius-time graph and its frequency response spectrum (such as ultra-harmonic and sub-harmonic components). Under these conditions, the bubble in the compression phase will experience the buckling state of the bubble shell due to the zero value of the surface tension. On the other hand, in the expansion phase of the bubble, the surface tension of the shell has increased rapidly, and this sudden change causes asymmetry in the bubble radial behavior in the radius-time graph. This phenomenon is called the compression-only behavior and was discovered by De Jong during the high-speed imaging of phospholipid-coated microbubbles. In the compression-only behavior, the changes of the bubble radial in the compression phase ( $\Delta R^- = R_0 - R_{\min}$ ) are greater than that in the expansion phase ( $\Delta R^+ = R_{\max} - R_0$ ). Only the nonlinear shell models can detect the compression-only behavior and the nonlinear bubble oscillation because they assume that the bubble shell behavior is physically different in the expansion and compression phase. In fact, the main disadvantage of the early models for the bubble dynamics is the linearity of their shell descriptors. Therefore, they are not capable to describe the nonlinear effects such as the compression-only behavior and the dependence of the shell material properties on the initial bubble radius. For this reason, a Marmottant nonlinear shell model is used here to investigate the nonlinear oscillation regime of the bubble.

According to Figures 7 and 8, and regarding the amplitude of excitation pressure and excitation frequency, the bubble experiences linear oscillations. Both the linear and nonlinear shell models used in this simulation have clearly shown the differences in the magnitude of bubble oscillation amplitude. The compression-only behavior is observed in the Marmottant nonlinear shell model, while the De Jong linear shell model does not predict it because the bubble buckling state is not considered in the compression phase. It can be seen that in the nonlinear shell model, the bubble oscillation amplitude is  $0.45 \mu\text{m}$  and the dimensionless parameter  $E/C$  (the ratio of expansion to the bubble compression) is  $0.5$ ; but in the linear shell model, these values are  $0.26 \mu\text{m}$  and  $1.15$ , respectively. In this case, except for the fundamental component ( $f_0$ )

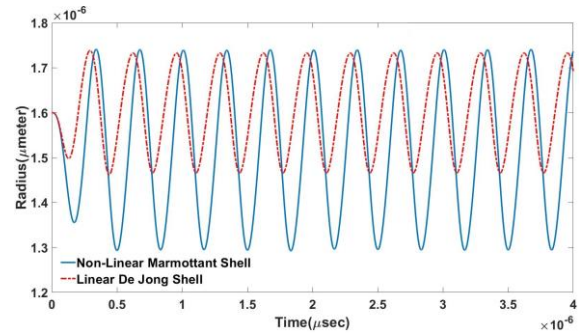


**Figure 7.** Radius-time curve for a  $1.6 \mu\text{m}$  Sonazoid bubble in the linear oscillation regime for the linear De Jong shell and the nonlinear Marmottant shell ( $P_a = 0.1 \text{ MPa}$ ,  $f = 3 \text{ MHz}$ )

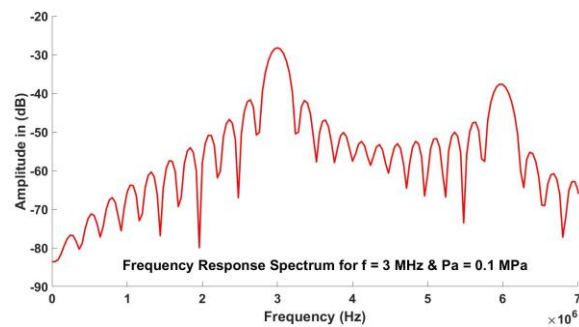


**Figure 8.** Frequency spectrum curve for a  $1.6 \mu\text{m}$  Sonazoid bubble in the linear oscillation regime ( $P_a = 0.1 \text{ MPa}$ ,  $f = 3 \text{ MHz}$ )

and the higher harmonics ( $2f_0$ ), no nonlinear component is seen in the bubble frequency response spectrum.

But, regarding Figures 9 and 10 and the nonlinear oscillation conditions for the bubble, it is observed that in addition to the asymmetry and nonlinearity of the bubble radial behavior in the frequency response spectrum, nonlinear components such as sub-harmonic ( $1/2 f_0$ ) and ultra-harmonic components ( $3/2 f_0$ ) have also appeared. It is also observed that the compression-only behavior disappears after a certain excitation pressure amplitude due to the rupturing of the bubble shell and the coated bubble becomes a free bubble. The shell rupture occurs due to violent bubble oscillations and high bubble expansions. Consequently, when the bubble surface tension is fixed ( $\sigma = \sigma_{\text{water}}$ ), the bubble no longer exhibits the compression-only behavior (since the variable surface tension in the Marmottant model plays a major role in the prediction of the compression-only behavior). Then, with increasing the excitation pressure amplitude, the bubble radius in the expansion phase becomes larger than the compression phase ( $\Delta R^+ > \Delta R^-$ ), in contrast to the compression-only behavior. When the excitation frequency increases, this behavior will be delayed by decreasing the mechanical index of the bubble ( $MI = P_a/\sqrt{f}$  where  $P_a$  is the amplitude of the excitation pressure

and  $f$  is the excitation frequency). Therefore, at higher excitation frequencies the compression-only behavior disappears at higher excitation pressure amplitudes.

Figures 11 shows the radius-time graphs for a coated bubble at two excitation frequencies of 3 MHz and 6 MHz and at different excitation pressure amplitudes. The linear and nonlinear changes in bubble oscillations can be studied using these figures. It is observed that the bubble oscillations near the elastic wall are more restricted than those in the infinite fluid, although for the lower excitation frequencies this radial oscillation suppression is more significant. It is also observed that as the excitation frequency increases, nonlinear bubble oscillation is suppressed and the bubble needs higher excitation pressure amplitude for nonlinear oscillations.

On the other hand, in the low excitation pressure amplitude the bubble oscillations are linear and at the same time the bubble experiences compression-only behavior. While, with increasing amplitude of excitation pressure, the bubble has nonlinear oscillations and the compression-only behavior is also disappeared. Also, as previously stated, by increasing the excitation frequency and consequently decreasing the mechanical index, the compression-only behavior of the bubble is delayed. For

more explanation, in Figures 11a to c with an excitation frequency of 3 MHz, the compression-only behavior gradually disappears with increasing the amplitude of excitation pressure; whereas, in Figures 11d to f with an excitation frequency of 6 MHz, with increasing excitation pressure amplitude the compression-only behavior is still observed.

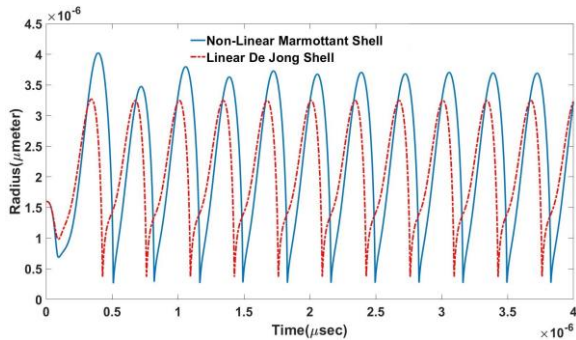


**Figure 9.** Radius-time curve for a 1.6  $\mu\text{m}$  Sonazoid bubble in the nonlinear oscillation regime for the linear De Jong shell and the nonlinear Marmottant shell ( $P_a = 1 \text{ MPa}$ ,  $f = 3 \text{ MHz}$ )

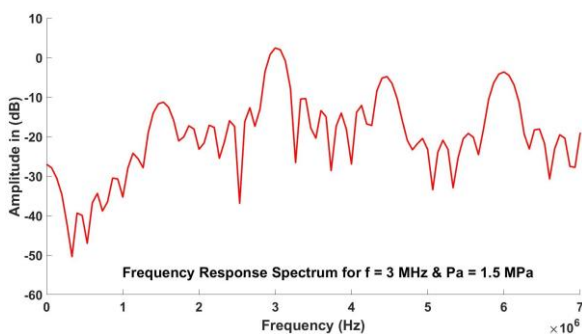
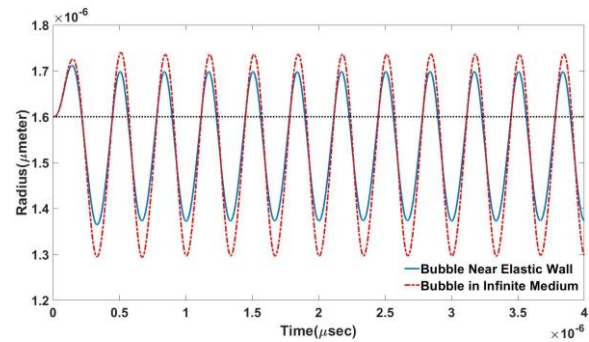
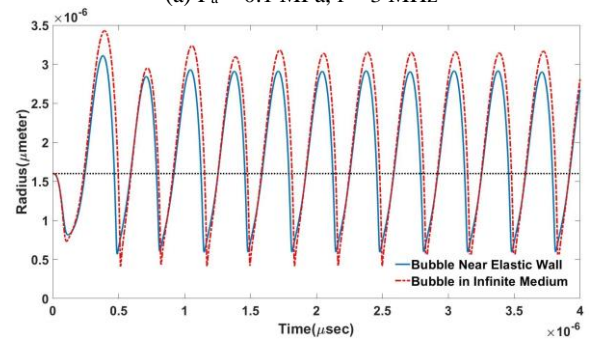


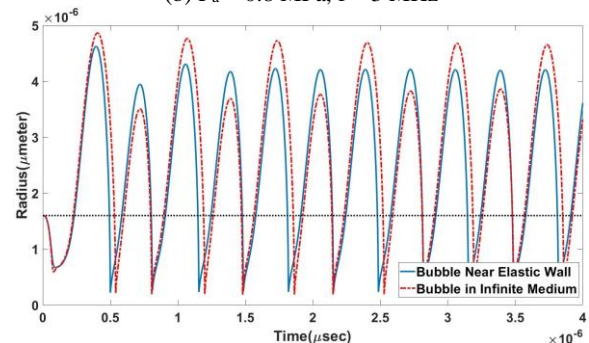
**Figure 10.** Frequency spectrum curve for a 1.6  $\mu\text{m}$  Sonazoid bubble in the nonlinear oscillation regime ( $P_a = 1 \text{ MPa}$ ,  $f = 3 \text{ MHz}$ )



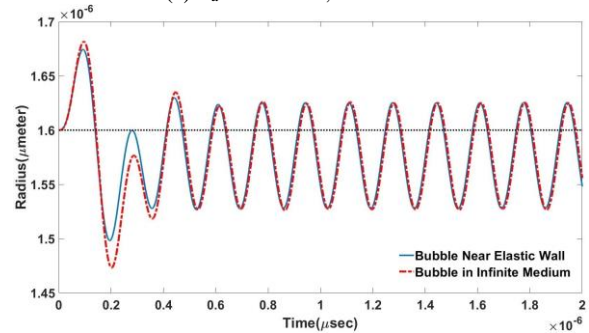
(a)  $P_a = 0.1 \text{ MPa}$ ,  $f = 3 \text{ MHz}$



(b)  $P_a = 0.8 \text{ MPa}$ ,  $f = 3 \text{ MHz}$



(c)  $P_a = 1.5 \text{ MPa}$ ,  $f = 3 \text{ MHz}$



(d)  $P_a = 0.1 \text{ MPa}$ ,  $f = 6 \text{ MHz}$

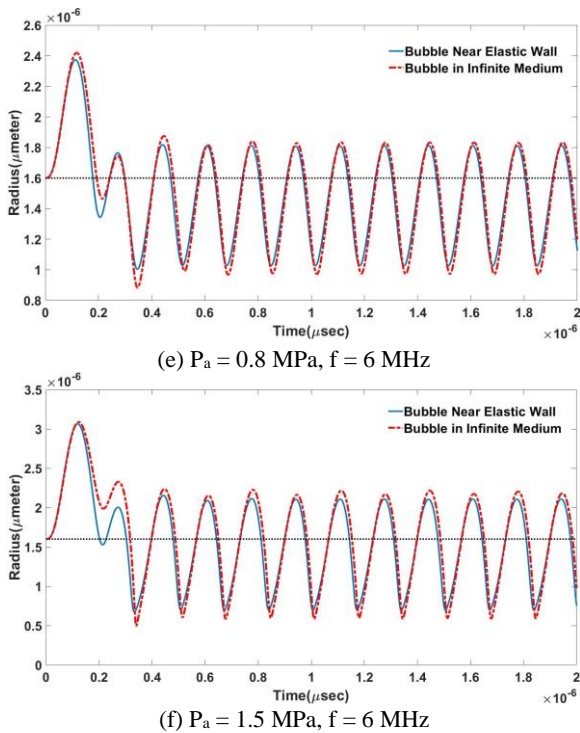


**Figure 11.** Radius-time curves for a  $1.6 \mu\text{m}$  Sonazoid bubble according to the presence of the wall

In the following, the compression-only behavior of the coated microbubble is investigated by the E/C dimensionless parameter in terms of different excitation pressure amplitudes. As shown in Figure 12, at a constant excitation frequency (3 MHz) and a constant excitation pressure amplitude, the bubble near the elastic wall has a less tendency to maintain the compression-only behavior. Hence, by increasing the amplitude of the excitation pressure from 0.1 to 1.6 MPa, the difference of the dimensionless E/C parameter between the two diagrams of the cases with and without wall increases from 0 to 0.619. In other words, the bubble shell when the bubble is oscillating near an elastic wall will rupture at lower pressure amplitude compared to oscillation in an infinite fluid. It may be due to the suppression of the bubble oscillations near the elastic wall. Oscillation of the bubble near a wall causes a reflected wave from the wall. This reflected wave suppresses bubble Oscillations and the bubble is less likely to retain the compression-only behavior. It is also seen in Figure 13 that for a coated bubble oscillating near an elastic wall, increasing the excitation pressure amplitude, as previously mentioned, attenuates the compression-only behavior, and whatever the excitation frequency will be higher, the disappearance of the compression-only behavior would be delayed. It can be seen that at the excitation frequency of 3 MHz, the compression-only behavior disappears at the excitation pressure of 0.5 MPa. While, at the excitation frequency of 6 MHz even at the excitation pressure amplitude of 1.6

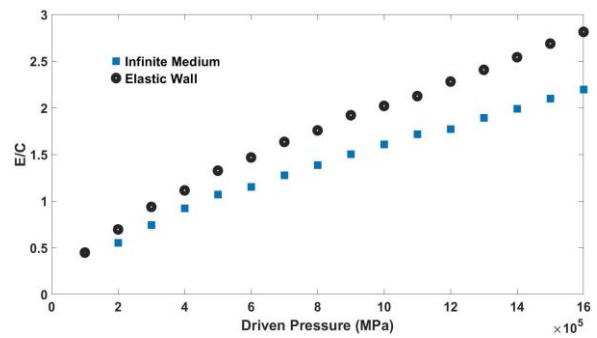


**Figure 12.** E/C values for a  $1.6 \mu\text{m}$  Sonazoid bubble as a function of excitation pressure in both cases, the bubble oscillates near an elastic wall and an infinite liquid ( $f = 3 \text{ MHz}$ )

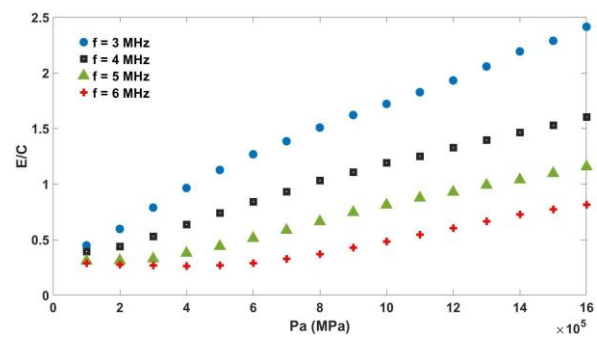


**Figure 13.** E/C values for a  $1.6 \mu\text{m}$  Sonazoid bubble as a function of excitation pressure at different frequency (in the case of the bubble oscillates near an elastic wall)

MPa this phenomenon still exists, and at the excitation pressure of 1.6 MPa and for both the excitation frequencies of 3 and 6 MHz, the difference of E/C parameter value is 1.6. Since by increasing the excitation frequency the nonlinear bubble oscillations are limited. Hence, rupturing of the bubble shell requires more excitation pressure amplitude, therefore, the compression-only behavior disappears.

### 3. 2. Investigation of the Frequency Response of Coated Bubble Near an Elastic Wall

In Section 3.2, the physical properties of both the bubble and wall and the nonlinear shell model are selected as before. The sub-harmonic components in modern medical imaging methods are so important, therefore their detection and prediction are imperative. On the other hand, the sub-harmonic components appear in the nonlinear bubble oscillation regime and accordingly at high excitation pressure amplitudes. These components will disappear after a critical excitation pressure amplitude and the bubble frequency-response spectrum will be saturated. Therefore, the nonlinear components cannot be distinguished from noise. Based on this, it is very important to determine the threshold of the excitation pressure amplitude.

In Figure 14, the sub-harmonic thresholds for a Sonazoid bubble with an initial radius of  $3\ \mu\text{m}$  and with similar physical properties to that of previously mentioned are given for two states of the nonlinear bubble oscillation near an elastic wall and an infinite fluid. In this graph, the sub-harmonic threshold value as a function of the excitation frequency divided by the bubble resonance frequency is investigated for the nonlinear Marmottant model. In the simulation process, the sub-harmonic components are not present at low excitation pressures, but with increasing the amplitude of the excitation pressure at a certain pressure value, the first sub-harmonics components will appear in the bubble frequency-response spectrum. In fact, the sub-harmonics thresholds occur at a certain value of excitation frequency within a particular excitation pressure range. The figure shows that at a given excitation frequency, the coated bubble near an elastic wall has a higher sub-harmonic threshold. It may be due to the effect of the reflected waves from the wall on the adjacent bubble that makes the bubble to be more resistant against nonlinearity than the bubbles in the infinite fluid. Therefore, the bubble requires more excitation pressure amplitude to produce sub-harmonic components. Thus, it can be concluded that the presence of a wall, in general, does not change the behavior of sub-harmonic components qualitatively, but in terms of quantitative measures, it will change (the sub-harmonic threshold level increases).

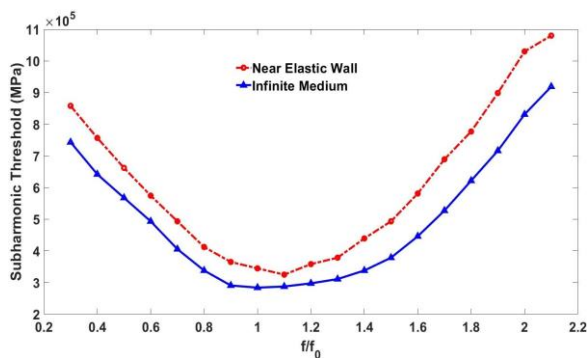


**Figure 14.** Subharmonic threshold curve for a  $3\ \mu\text{m}$  Sonazoid bubble in both cases, the bubble oscillates near an elastic wall and an infinite liquid

#### 4. CONCLUSION

In this paper, the nonlinear behavior of a coated microbubble with a focus on the proximity of an elastic wall is investigated. Initially, as the ability of the selected shell model to predict the nonlinear components is crucial, the effect of the selective shell model on the simulation results for a coated bubble near the elastic wall was investigated using both the De Jong linear shell model and the Marmottant nonlinear shell model. It was

found that both models well described the compression-only behavior and difference in the bubble oscillation amplitude. Then, due to the importance of nonlinear bubble oscillations in medical applications, the oscillations of a bubble near an elastic wall in several different excitations have been studied to investigate the nonlinear behavior of the bubble and its compression-only behavior. It was observed that the bubble near the elastic wall is less prone to maintain the compression-only behavior than the bubble in the infinite fluid, and change in the excitation frequency can delay the disappearance of the compression-only behavior. As the excitation pressure amplitude increased from 0.1 to 1.6 MPa, the difference between the two diagrams in the dimensionless  $E/C$  parameter in both with and without wall cases enlarged from 0 to 0.619. It was also found that for the bubble oscillation near the elastic wall, with increasing excitation pressure amplitude the intensity of compression-only behavior of the bubble weakened, and whenever the excitation frequency was higher, the disappearance of the compression-only behavior was delayed. Furthermore, because there is a great deal of focus on sub-harmonic components in modern medical imaging techniques, the sub-harmonic threshold has been investigated. Investigations showed that at a given excitation frequency, the coated bubble near an elastic wall has a higher sub-harmonic threshold than the bubble in the infinite fluid.

#### 5. REFERENCES

- De Jong, N., Hoff, L., Skotland, T., and Bom, N. "Absorption and scatter of encapsulated gas filled microspheres: Theoretical considerations and some measurements." *Ultrasonics*, Vol. 30, No. 2, (1992), 95–103. [https://doi.org/10.1016/0041-624X\(92\)90041-J](https://doi.org/10.1016/0041-624X(92)90041-J)
- Church, C. C. "The effects of an elastic solid surface layer on the radial pulsations of gas bubbles." *Journal of the Acoustical Society of America*, Vol. 97, No. 3, (1995), 1510–1521. <https://doi.org/10.1121/1.412091>
- Hoff, L., Sontum, P. C., and Hovem, J. M. "Oscillations of polymeric microbubbles: Effect of the encapsulating shell." *The Journal of the Acoustical Society of America*, Vol. 107, No. 4, (2000), 2272–2280. <https://doi.org/10.1121/1.428557>
- De Jong, N., Bouakaz, A., and Frinking, P. "Basic acoustic properties of microbubbles." *Echocardiography*. Vol. 19, No. 3, (2002), 229–240. <https://doi.org/10.1046/j.1540-8175.2002.00229.x>
- Brennen, C. Cavitation and bubble dynamics. Oxford University Press, (1995).
- Leighton, T. G. "The inertial terms in equations of motion for bubbles in tubular vessels or between plates." *The Journal of the Acoustical Society of America*, Vol. 130, No. 5, (2011), 3333–3338. <https://doi.org/10.1121/1.3638132>
- Blake, J. R., and Gibson, D. C. "Cavitation Bubbles Near Boundaries." *Annual Review of Fluid Mechanics*, Vol. 19, No. 1, (1987), 99–123. <https://doi.org/10.1146/annurev.fl.19.010187.000531>
- Herring, C. "Theory of the pulsations of the gas bubble produced

- by an underwater explosion." In Technical Report 236, Columbia University, Division of National Defense Research, (1941).
9. Strasberg, M. "The Pulsation Frequency of Nonspherical Gas Bubbles in Liquids." *Journal of the Acoustical Society of America*, Vol. 25, No. 3, (1953), 536-537. <https://doi.org/10.1121/1.1907076>
  10. Blue, J. E. "Resonance of a Bubble on an Infinite Rigid Boundary." *The Journal of the Acoustical Society of America*, Vol. 41, No. 2, (1967), 369-372. <https://doi.org/10.1121/1.1910347>
  11. Doinikov, A. A., Zhao, S., and Dayton, P. A. "Modeling of the acoustic response from contrast agent microbubbles near a rigid wall." *Ultrasonics*, Vol. 49, No. 2, (2009), 195-201. <https://doi.org/10.1016/j.ultras.2008.07.017>
  12. Tomita, Y., and Shima, A. "Mechanisms of impulsive pressure generation and damage pit formation by bubble collapse." *Journal of Fluid Mechanics*, Vol. 169, (1986), 535-564. <https://doi.org/10.1017/S0022112086000745>
  13. Doinikov, A. A., Aired, L., and Bouakaz, A. "Acoustic response from a bubble pulsating near a fluid layer of finite density and thickness." *The Journal of the Acoustical Society of America*, Vol. 129, No. 2, (2011), 616-621. <https://doi.org/10.1121/1.3531839>
  14. Garbin, V., Cojoc, D., Ferrari, E., Di Fabrizio, E., Overvelde, M. L. J., Van Der Meer, S. M., De Jong, N., Lohse, D., and Versluis, M. "Changes in microbubble dynamics near a boundary revealed by combined optical micromanipulation and high-speed imaging." *Applied Physics Letters*, Vol. 90, No. 11, (2007), 114103. <https://doi.org/10.1063/1.2713164>
  15. Doinikov, A. A., and Bouakaz, A. "Interaction of an ultrasound-activated contrast microbubble with a wall at arbitrary separation distances." *Physics in Medicine and Biology*, Vol. 60, No. 20, (2015), 7909-7925. <https://doi.org/10.1088/0031-9155/60/20/7909>
  16. Overvelde, M., Garbin, V., Dollet, B., De Jong, N., Lohse, D., and Versluis, M. "Dynamics of Coated Microbubbles Adherent to a Wall." *Ultrasound in Medicine and Biology*, Vol. 37, No. 9, (2011), 1500-1508. <https://doi.org/10.1016/j.ultrasmedbio.2011.05.025>
  17. Aired, L., Doinikov, A. A., and Bouakaz, A. "Effect of an elastic wall on the dynamics of an encapsulated microbubble: A simulation study." *Ultrasonics*, Vol. 53, No. 1, (2013), 23-28. <https://doi.org/10.1016/j.ultras.2012.03.008>
  18. Garashchuk, I. R., Sinelshchikov, D. I., and Kudryashov, N. A. "Nonlinear Dynamics of a Bubble Contrast Agent Oscillating near an Elastic Wall." *Regular and Chaotic Dynamics*, Vol. 23, No. 3, (2018), 257-272. <https://doi.org/10.1134/S1560354718030036>
  19. Paul, S., Katiyar, A., Sarkar, K., Chatterjee, D., Shi, W. T., and Forsberg, F. "Material characterization of the encapsulation of an ultrasound contrast microbubble and its subharmonic response: Strain-softening interfacial elasticity model." *The Journal of the Acoustical Society of America*, Vol. 127, No. 6, (2010), 3846-3857. <https://doi.org/10.1121/1.3418685>
  20. Paul, S. "Acoustic characterization of ultrasound contrast microbubbles and echogenic liposomes: applications to imaging and drug-delivery", Doctoral Dissertations, University of Delaware, USA, (2013). Retrieved from <https://udspace.udel.edu/handle/19716/20934>
  21. Marmottant, P., van der Meer, S., Emmer, M., Versluis, M., de Jong, N., Hilgenfeldt, S., and Lohse, D. "A model for large amplitude oscillations of coated bubbles accounting for buckling and rupture." *The Journal of the Acoustical Society of America*, Vol. 118, No. 6, (2005), 3499-3505. <https://doi.org/10.1121/1.2109427>
  22. Löfstedt, R., Barber, B. P., and Putterman, S. J. "Toward a hydrodynamic theory of sonoluminescence." *Physics of Fluids A*, Vol. 5, No. 11, (1992), 2911-2928. <https://doi.org/10.1063/1.858700>

---

### Persian Abstract

#### چکیده

از آن جا که در فرایند تصویربرداری فراصوتی عوامل تقابلی فراصوتی در حال ضربان در مجاورت دیواره‌ی رگ خونی هستند، هدف این پژوهش مطالعه‌ی شبیه‌سازی حاضر این است که بررسی کنیم چگونه حضور یک دیواره‌ی کش‌سان بر پاسخ آکوستیک شعاعی و فرکانسی یک میکروحباب عامل تقابلی فراصوتی که در حال نوسان در یک رژیم غیرخطی است، تاثیر می‌گذارد. به همین دلیل در این مقاله شبیه‌سازی عددی رفتار دینامیک یک میکروحباب پوشش‌دار با استفاده از کدنویسی در متلب و یک معادله رایلی-پلیست اصلاح شده توسط دوینیکف انجام شده است. به‌منظور بررسی نوسانات غیرخطی حباب، رفتار انقباض غالب آن و مولفه غیرخطی زیرهارمونیک از یک مدل پوسته‌ی غیرخطی که توسط مارمونت و همکاران ارائه شده، بهره گرفته شده است. ابتدا نوسانات حباب پوشش‌دار در دو رژیم خطی و غیرخطی برای دو نوع مدل پوسته بررسی شده است. درنهایت، به دلیل اهمیت مولفه‌ی زیرهارمونیک در نوسان غیرخطی حباب پوشش‌دار با استفاده از تبدیل فوریه (FFT) آستانه‌ی ظهور مولفه‌های زیرهارمونیک برای یک حباب پوشش‌دار در نزدیکی یک دیواره‌ی کش‌سان بررسی گردیده و با حالت نوسان در مایع بی‌کران مقایسه شده است.

---